136

SATELLITE & MESOMETEOROLOGY RESEARCH PROJECT

Department of the Geophysical Sciences
The University of Chicago

CLOUD-MOTION VECTORS OVER THE GATE AREA COMPUTED BY McIDAS AND METRACOM METHODS

by

Jaime J. Tecson and T. Theodore Fujita

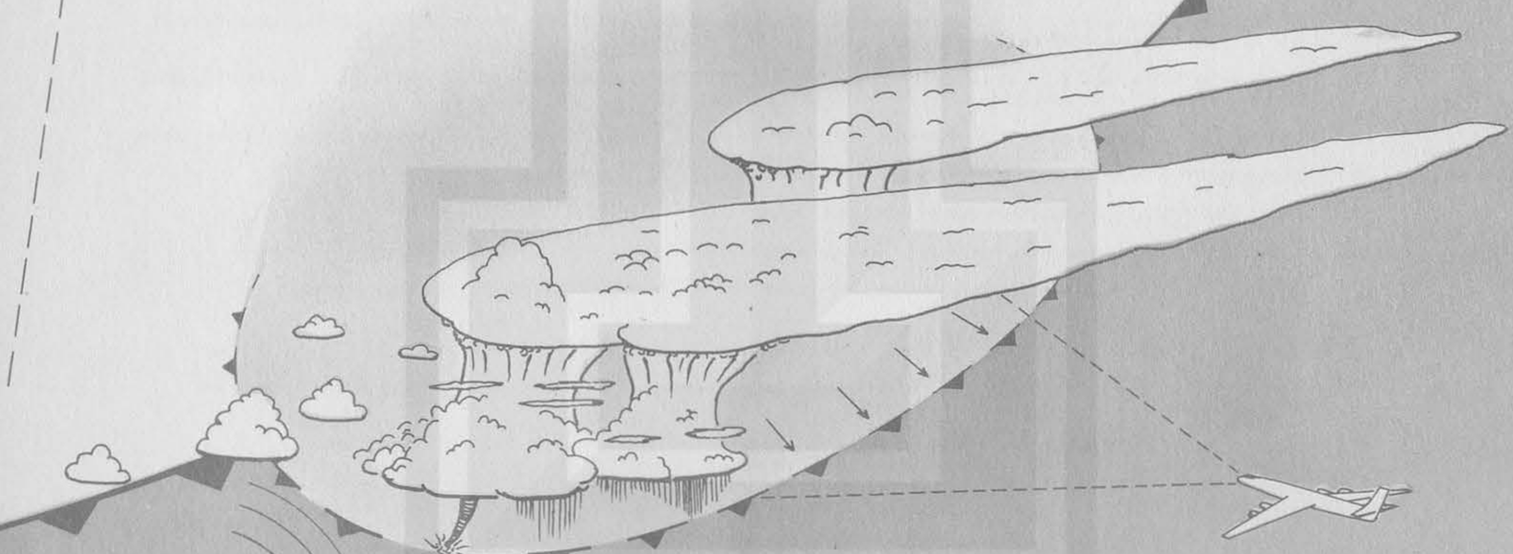

SMRP Research Paper No. 136
December 1975

MESOMETEOROLOGY PROJECT --- RESEARCH PAPERS

1.* Report on the Chicago Tornado of March 4, 1961 - Rodger A. Brown and Tetsuya Fujita

2.* Index to the NSSP Surface Network - Tetsuya Fujita

3.* Outline of a Technique for Precise Rectification of Satellite Cloud Photographs - Tetsuya Fujita

4.* Horizontal Structure of Mountain Winds - Henry A. Brown

5.* An Investigation of Developmental Processes of the Wake Depression Through Excess Pressure Analysis of Nocturnal Showers - Joseph L. Goldman

6.* Precipitation in the 1960 Flagstaff Mesometeorological Network - Kenneth A. Styber

7.** On a Method of Single- and Dual-Image Photogrammetry of Panoramic Aerial Photographs - Tetsuya Fujita

8. A Review of Researches on Analytical Mesometeorology - Tetsuya Fujita

9.* Meteorological Interpretations of Convective Nephsystems Appearing in TIROS Cloud Photographs - Tetsuya Fujita, Toshimitsu Ushijima, William A. Hass, and George T. Dellert, Jr.

10.* Study of the Development of Prefrontal Squall-Systems Using NSSP Network Data - Joseph L. Goldman

11. Analysis of Selected Aircraft Data from NSSP Operation, 1962 - Tetsuya Fujita

12. Study of a Long Condensation Trail Photographed by TIROS I - Toshimitsu Ushijima

13. A Technique for Precise Analysis of Satellite Data; Volume I - Photogrammetry (Published as MSL Report No. 14) - Tetsuya Fujita

14. Investigation of a Summer Jet Stream Using TIROS and Aerological Data - Kozo Ninomiya

15. Outline of a Theory and Examples for Precise Analysis of Satellite Radiation Data - Tetsuya Fujita

16. Preliminary Result of Analysis of the Cumulonimbus Cloud of April 21, 1961 - Tetsuya Fujita and James Arnold

17. A Technique for Precise Analysis of Satellite Photographs - Tetsuya Fujita

18.* Evaluation of Limb Darkening from TIROS III Radiation Data - S.H.H. Larsen, Tetsuya Fujita, and W.L. Fletcher

19. Synoptic Interpretation of TIROS III Measurements of Infrared Radiation - Finn Pedersen and Tetsuya Fujita

20.* TIROS III Measurements of Terrestrial Radiation and Reflected and Scattered Solar Radiation - S.H.H. Larsen, Tetsuya Fujita, and W.L. Fletcher

21. On the Low-level Structure of a Squall Line - Henry A. Brown

22.* Thunderstorms and the Low-level Jet - William D. Bonner

23.* The Mesoanalysis of an Organized Convective System - Henry A. Brown

24. Preliminary Radar and Photogrammetric Study of the Illinois Tornadoes of April 17 and 22, 1963 - Joseph L. Goldman and Tetsuya Fujita

25. Use of TIROS Pictures for Studies of the Internal Structure of Tropical Storms - Tetsuya Fujita with Rectified Pictures from TIROS I Orbit 125, R/O 128 - Toshimitsu Ushijima

26. An Experiment in the Determination of Geostrophic and Isallobaric Winds from NSSP Pressure Data - William Bonner

27. Proposed Mechanism of Hook Echo Formation - Tetsuya Fujita with a Preliminary Mesosynoptic Analysis of Tornado Cyclone Case of May 26, 1963 - Tetsuya Fujita and Robbi Stuhmer

28. The Decaying Stage of Hurricane Anna of July 1961 as Portrayed by TIROS Cloud Photographs and Infrared Radiation from the Top of the Storm - Tetsuya Fujita and James Arnold

29. A Technique for Precise Analysis of Satellite Data, Volume II - Radiation Analysis, Section 6. Fixed-Position Scanning - Tetsuya Fujita

30. Evaluation of Errors in the Graphical Rectification of Satellite Photographs - Tetsuya Fujita

31. Tables of Scan Nadir and Horizontal Angles - William D. Bonner

32. A Simplified Grid Technique for Determining Scan Lines Generated by the TIROS Scanning Radiometer - James E. Arnold

33. A Study of Cumulus Clouds over the Flagstaff Research Network with the Use of U-2 Photographs - Dorothy L. Bradbury and Tetsuya Fujita

34. The Scanning Printer and Its Application to Detailed Analysis of Satellite Radiation Data - Tetsuya Fujita

35. Synoptic Study of Cold Air Outbreak over the Mediterranean using Satellite Photographs and Radiation Data - Aasmund Rabbe and Tetsuya Fujita

36. Accurate Calibration of Doppler Winds for their use in the Computation of Mesoscale Wind Fields - Tetsuya Fujita

37. Proposed Operation of Intrumented Aircraft for Research on Moisture Fronts and Wake Depressions - Tetsuya Fujita and Dorothy L. Bradbury

38. Statistical and Kinematical Properties of the Low-level Jet Stream - William D. Bonner

39. The Illinois Tornadoes of 17 and 22 April 1963 - Joseph L. Goldman

40. Resolution of the Nimbus High Resolution Infrared Radiometer - Tetsuya Fujita and William R. Bandeen

41. On the Determination of the Exchange Coefficients in Convective Clouds - Rodger A. Brown

* Out of Print
** To be published

(Continued on back cover)

CLOUD-MOTION VECTORS OVER THE GATE AREA COMPUTED BY McIDAS AND METRACOM METHODS

by

Jaime J. Tecson and T. Theodore Fujita
Department of the Geophysical Sciences
The University of Chicago

SMRP Research Paper No. 136
December 1975

This research was supported by the Atmospheric Sciences Section, National Science Foundation grant DES 74-08119A01 and in part by the National Oceanic and Atmospheric Administration under grant 04-4-158-1 and the National Aeronautics and Space Administration under grant NGR 14-001-008.

CLOUD-MOTION VECTORS OVER THE GATE AREA COMPUTED BY McIDAS AND METRACOM METHODS

by

Jaime J. Tecson and T. Theodore Fujita
Department of the Geophysical Sciences
The University of Chicago

ABSTRACT

Computations of cloud-motion vectors over the area of the GARP Atlantic Tropical Experiment (GATE) A/B-scale ship network on a specified time were performed independently by the University of Wisconsin using its Man-Computer Interactive Data Access System (McIDAS) and by the University of Chicago through its METeorologist-TRAcking-COMputer (METRACOM) Interactive System.

It was intended to assess the results of these techniques using picture images with identical image subpoint resolution and time-interval frequency. However, McIDAS utilized the finest-resolution and shortest-interval film images with processing done on original digitized data, while METRACOM used the larger-resolution and longer-interval pictures only available then. Results showed that picture resolution and time-interval factors are very important.

Fine-resolution ungridded pictures were subsequently obtained from the National Climatic Center. In evaluating the data, it was observed that picture skewness of irregular magnitudes characterized the series. Finding no way to correct it, and inasmuch as the

METRACOM technique uses high-quality, dimension-controlled pictures as input, it was considered inappropriate to compare the two methods.

Nevertheless, the results of the analyses are discussed.

INTRODUCTION

One of the scientific objectives of the GARP Atlantic Tropical Experiment (GATE) during the period June through September, 1974, although not within the Central Program, was "the provision of data for intercomparison between satellite and conventional observations" (Houghton and Parker, 1974). The enhanced tropical data network available in this period provided a unique opportunity to attain this objective. The data-gathering resources of the participating international scientific community consisted mainly of observations from GATE ships and aircraft, World Weather Watch land stations and meteorological satellites. Of the types of satellites employed, quite an important aspect has been contributed by the first Synchronous Meteorological Satellite (SMS-1) from which, in areas where clouds are present, cloud motions can be computed at frequent intervals in the determination of the upper winds. Throughout GATE the SMS-1 geostationary spacecraft was positioned at approximately 45°W over the equator. Imaging was accomplished by a visible and infrared spin scan radiometer (VISSR), sensitive to both visible and infrared portions of the spectrum (ISMG Group, 1975). Of significance is the fact that, for the first time, a 0.5-nautical-mile range resolution (nmr) on the earth's surface at the subsatellite point is obtained by the visible channel.

It was, therefore, considered timely to assess the results of the computations of cloud-motion vectors using the Man-Computer Interactive Data Access System (McIDAS) developed at the University of Wisconsin (Martin, 1974) and the METeorologist-TRAcking-COMputer (METRACOM) Interactive System devised by the University of Chicago. Picture images with identical image subpoint resolution and time-interval frequency were intended to be used in both analyses over a common area in the GATE network and on a specified time. Hence, if the test results would be satisfactory and meet the requirements of GATE, it could then become possible for numerous analyses to be accomplished and more wind sets derived by the combined outputs of the two methods than if it were done by only one.

Considering such factors as density of the wind-observing network, cloud population, picture alignment accuracies, picture quality and availability, it was decided to jointly and independently track an area within the GATE A/B-scale ship network, bounded by 4° and 13°N and 18° and 29°W, at a centered time of 1500 GMT (Z) on 10 September 1974, one of the five days in GATE where 15-minute interval pictures were taken by SMS-1.

METHODS AND DATA AVAILABILITY

The cloud tracking system of McIDAS utilizes an image storage, display and processing system where the data is archived, accessed, video displayed, computer controlled and processed. All processing is done on original digital data. Tracking is performed on visible images using manually controlled cursor (pixel tracking) as it follows a tracer cloud from one picture displayed on the TV screen to the next. Together with a set of physical parameters determined by the orbital configuration of the satellite at the particular time, a computer program generates transformations from image coordinates to earth coordinates and vice versa. For more details and a complete description of McIDAS, refer to Suomi (1975), Chatters and Suomi (1975) and Smith (1975).

The cloud computation scheme of METRACOM consists initially of tracking a tracer cloud from a movie loop composed of a set of pictures in the visible channel projected onto an opaque working surface. The initial and terminal points of each cloud vector thus traced is transformed into Cartesian coordinates through a digitizer facility. These coordinate points automatically become input data to a computer program, which, together with other satellite orbital parameters and correction factors, outputs cloud vector location (geographical latitude and longitude of the beginning and end points) and velocity (azimuth and speed). A complete discussion of METRACOM is found in Chang *et al.* (1973).

McIDAS processed from its archive the original digital data for the 0.5 nmr image taken at 15-minute intervals using a three-picture sequence beginning at 1445 Z, a time period of one-half hour. Cloud motion computations were derived from that source. Figure 1 shows a sample photograph, reduced from 25 x 23 cm original size, of the 0.5 nmr visible channel picture at 1500 Z, 10 September 1974 (Day 253) over the GATE A/B area. The west coast of Africa with Dakar at the westernmost tip is seen at the upper-right section. The center of the A/B-scale ship array is located approximately at the lower third of the picture but otherwise centered in the east-west orientation. Meanwhile, efforts had been unsuccessful in obtaining 0.5 nmr visible pictures for the METRACOM analysis. As the only alternative, it was necessary to utilize the 2.0 nmr full-disk, 30-minute interval visible pictures for computing cloud motions while waiting for availability of the 0.5 nmr film images. A series of three pictures was used beginning at 1430 Z; the period covered one hour.

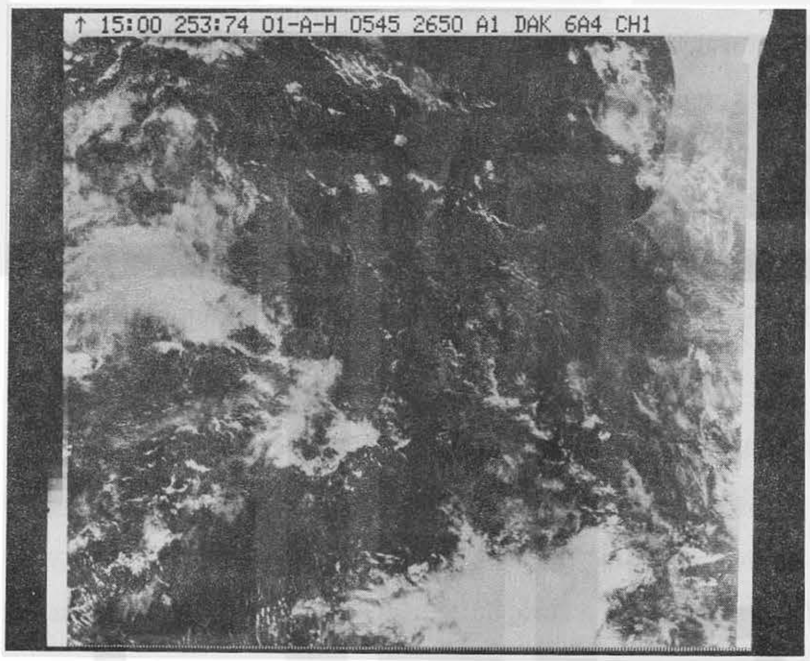

Fig. 1. A 0.5 nmr visible channel picture at 1500Z, 10 Sept. 1974 over the GATE A/B area. Dakar is at the protruding tip of the West African coast.

Figure 2 is a 2.0 nmr full-disk visible picture at 1500 Z on 10 September 1974 (Day 253), reduced from 25 x 18 cm original size. Without degrading picture quality, a movie loop was prepared from the zoom area shown as the largest rectangle (A). Cloud tracking was consequently confined therein. For comparison purposes, the next smaller rectangle (B) best approximates the area coverage of the corresponding 0.5 nmr visible picture (see Fig. 1). The smallest rectangle or square (C) indicates the common area of analysis by the McIDAS and METRACOM techniques.

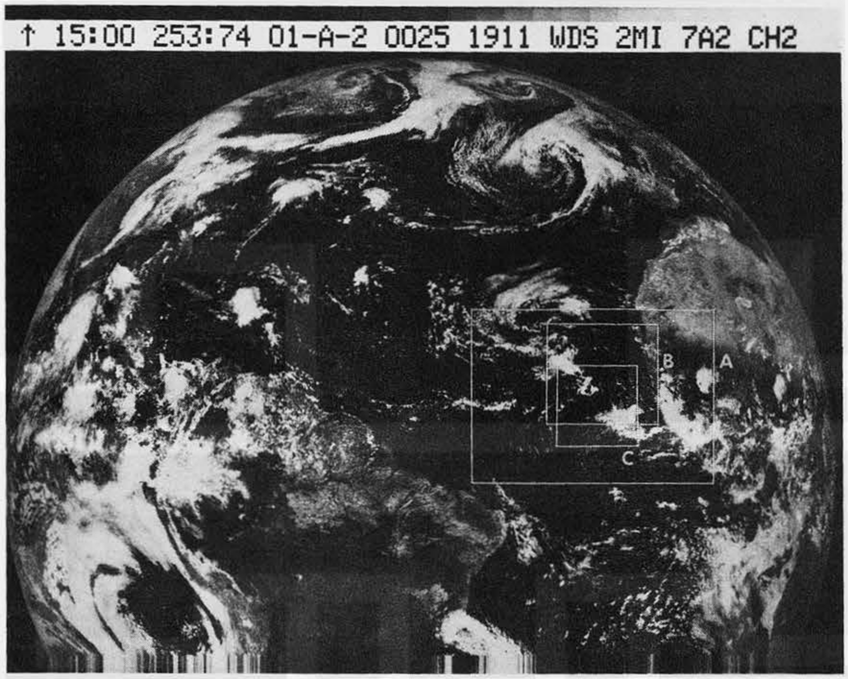

Fig. 2. A 2.0 nmr full-disk visible channel picture at 1500Z, 10 Sept. 1974. Rectangle B corresponds to Fig. 1.

Figure 3 shows the overall area of the METRACOM analysis. This corresponds to region A in Fig. 2. The rectangular shaded portion enclosing the imaginary outer hexagon of the A/B-scale ships is the region analyzed by the McIDAS system; hence, the common analysis area. It is also the region C in Fig. 2. Also shown in Fig. 3 are the locations of the GATE ships and participating land stations indicating available wind observations at various levels which were utilized in the comparison with the subjectively assigned levels of the cloud-motion vectors.

A more coherent cloud-motion pattern is presented if at least two levels, one for the lower (Fig. 4) and one for the upper troposphere cloud (Fig. 5) are drawn separately for the area of the METRACOM analysis averaged for the period 1430-1530 Z for 10 September 1974. Wind speeds are in knots. Interpolated 1500 Z winds from observations at 1200 Z and 1800 Z are plotted as applicable. Two levels of wind are

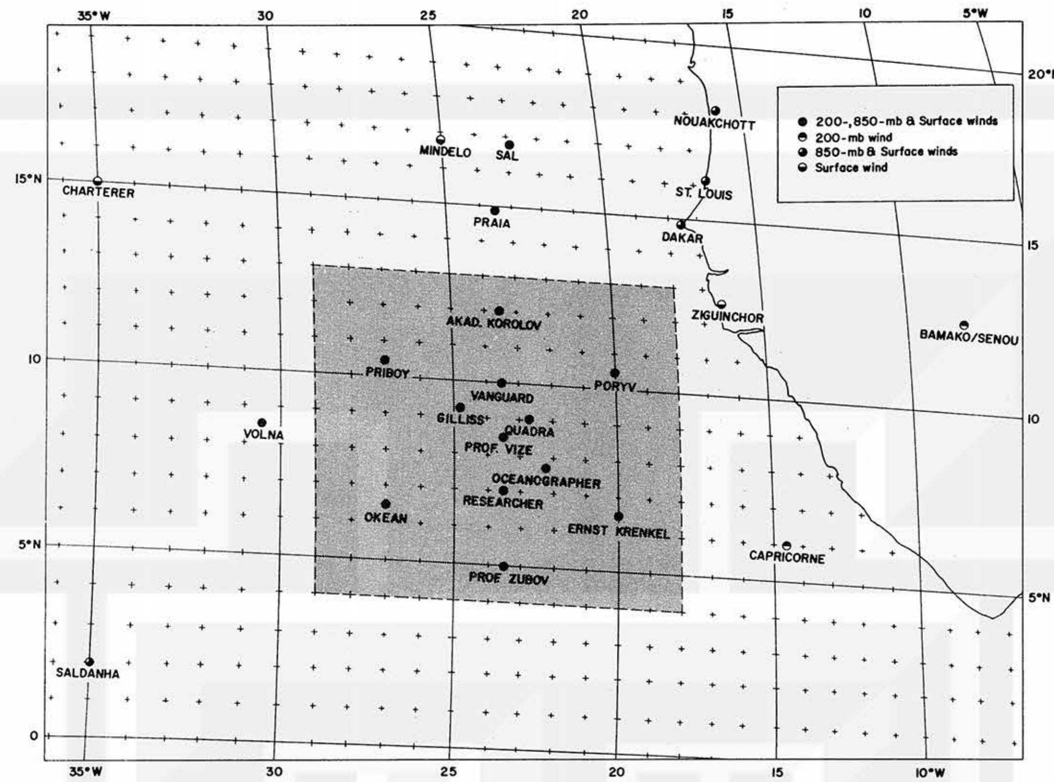

Fig. 3. GATE ships and land stations indicating available wind observations at 1200Z and/or 1800Z, 10 Sept. 1974. METRACOM analysis covers whole area; shaded portion is the common analysis area.

plotted in Fig. 4; one for 850-mb and the other for the surface. In regard to the surface winds, the level corresponds to that of the sea surface for ship observations and for 500/600 meter data for land station observations. Altogether a total of 358 cloud vectors were produced. In Fig. 5 the high-cloud vectors are indicated. Although an attempt is made to eliminate middle clouds from the analysis it is probable that the middle clouds could also have been traced. They total 160 vectors. Superimposed are the significant cloud configurations. The wind observations plotted are at the 200-mb level.

The wind conditions at the common analysis area at 1500 Z, deduced from the 1200 Z and 1800 Z observations on 10 September 1974, indicated that, at the lowest levels, the area was dominated by weak anticyclonic flow of about 5 knots. At the surface, it was influenced by the northwestern sector of the anticyclone and by the northeastern portion at 850-mb. At the 200-mb level, the wind flow was northeast averaging 37 knots.

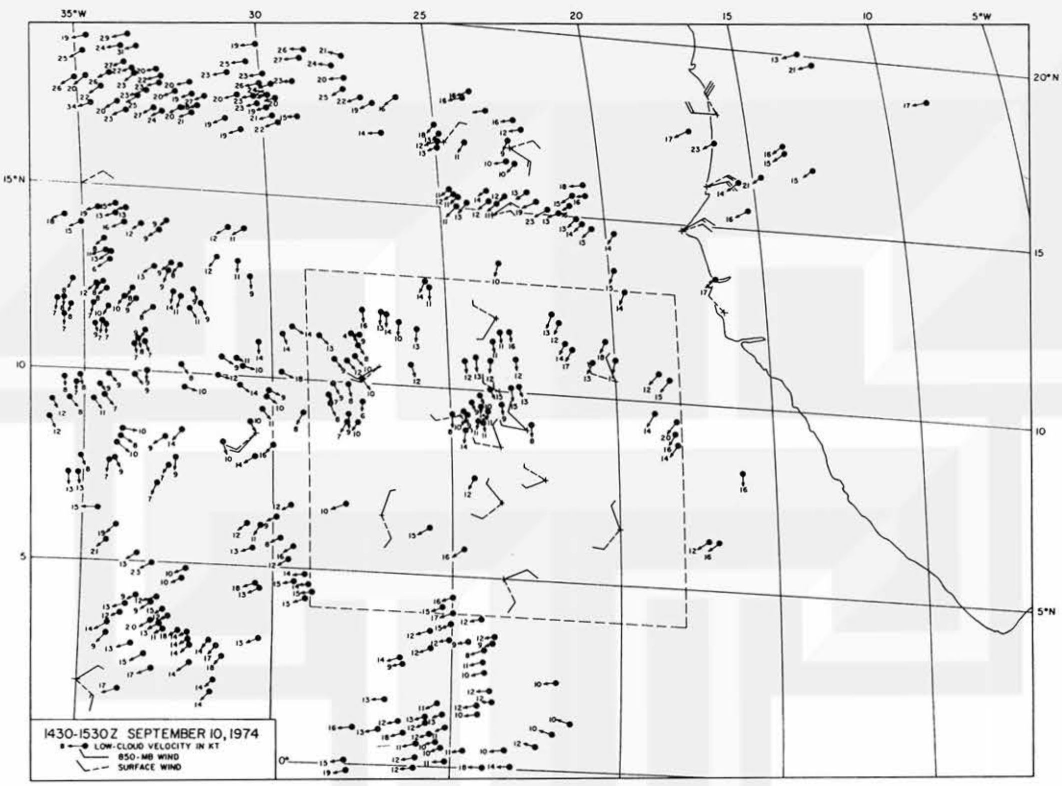

Fig. 4. Low-cloud velocity vectors, total 358, for the period 1430-1530Z, 10 Sept. 1974 computed by METRACOM technique. 1500Z or synoptic-time winds are plotted for the surface and 850-mb.

Table 1 summarizes the ship and land stations from which wind observations at various levels at the time indicated are compared with those of the surrounding satellite-derived cloud motions. Whenever it was not possible to interpolate the 1500 Z winds, either of the synoptic-time observations, except calm, is substituted. From a listing of locations and cloud velocities, time averaged at 1500 Z on 10 September 1974, produced by McIDAS (Martin, 1974), two charts are prepared using the identical type map and scale as that used in METRACOM in the two immediately preceding figures.

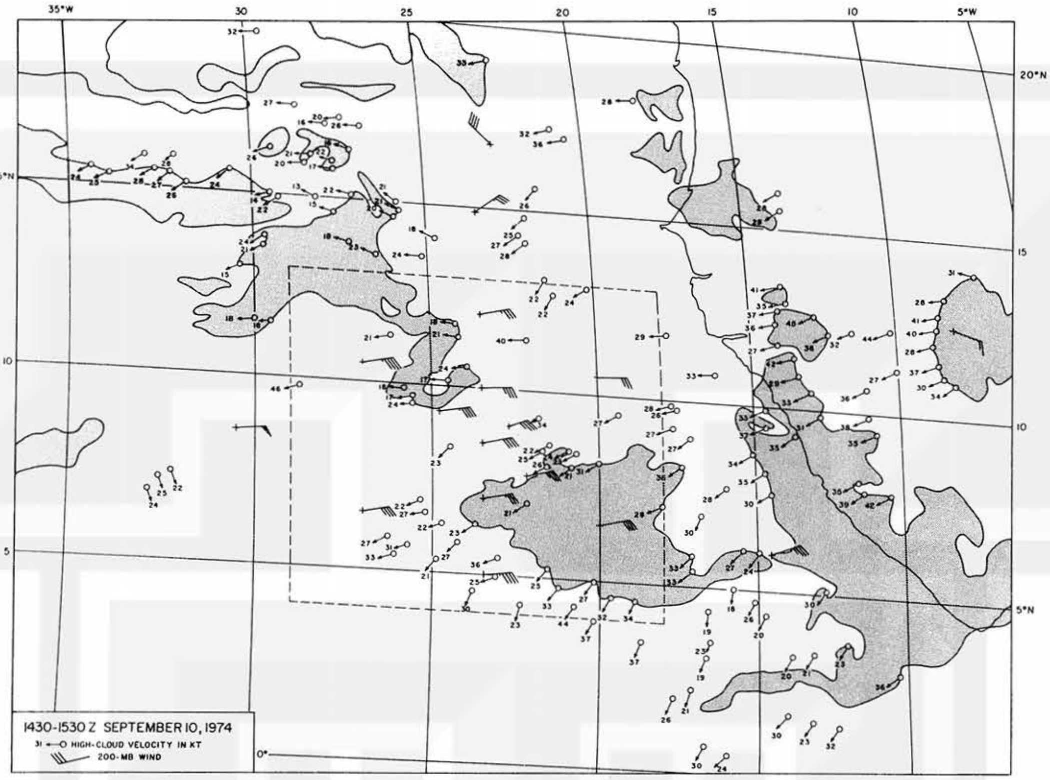

Fig. 5. As in Fig. 4 except for high-clouds, total 260, computed by METRACOM technique. Superimposed are significant cloud configurations. Winds plotted are at 200-mb level.

Figure 6 shows the low-cloud velocity vectors, which number 140, together with the 1500 Z winds at 850-mb and at the surface plotted in appropriate locations. There are only 69 vectors tracked by METRACOM in the same area. Similarly, Fig. 7 shows the upper troposphere cloud velocity vectors with the 200-mb winds included. Distinction is made between middle- and high-cloud vectors, each totalling 30 and 51, respectively. Correspondingly, there are 69 cloud vectors traced by the METRACOM system at this level.

Comparison of the low-cloud velocity vectors within the common analysis area would show discrepancies in cloud motions. These could possibly be due to differences in the levels of the low-clouds detected and tracked when the same area is analyzed from pictures taken with different ground resolution cameras. The 0.5 nmr pictures

Table 1. Summary of Reporting Stations and Reference Wind Observations on 10 September 1974.

NAME	Call Letter or Station Number	POSITION		WIND VELOCITY (ddd/ff)***								
				Ocean/Land**			8 5 0 - M B			2 0 0 - M B		
		° N	° W	1200Z	1500Z*	1800Z	1200Z	1500Z*	1800Z	1200Z	1500Z*	1800Z
A. GATE SHIPS												
Charterer	GTUC	15.0	35.0		060/11							
Akad. Korolov	UHQS	12.0	23.5		300/04			215/05			077/32	
Priboy	EREH	10.5	27.0	230/08				240/09			080/42	
Poryv	ERES	10.5	20.0		285/10			340/05			085/28	
Vanguard	MVAN	10.0	23.5		295/08			295/07			087/38	
Gilliss	WEWP	9.3	24.8		260/07			130/02			080/41	
Quadra	CGDN	9.0	22.7		280/05		315/09			070/37		
Volna	EREB	8.5	30.5		230/08			225/08			085/51	
Prof. Vize	UPUI	8.5	23.5		280/04			340/06			077/40	
Oceanographer	WTEP	7.7	22.2	300/02				250/05			075/35	
Researcher	WTER	7.0	23.5			230/08		320/05			080/31	
Okean	EREI	6.5	27.0		155/08		020/04				082/39	
Ernst Krenkel	EREU	6.5	20.0		220/08			340/04			077/40	
Capricorne	FNBG	6.0	14.5							070/37		
Prof. Zubov	UMFW	5.0	23.5		155/09			067/08			085/41	
Saldanha	PXSA	2.0	35.0	130/12					055/04			
B. LAND STATIONS												
Nouakchott	442	18.1	15.9			330/30			270/20			
Mindelo	583	16.9	25.0	040/04								
Sal	594	16.7	22.9	070/08			120/04			315/40		
Saint-Louis	600	16.1	16.5		060/19			075/18				
Praia	589	14.9	23.5	075/04			055/12			055/32		
Dakar	641	14.7	17.5	070/10				060/13				
Ziguinchor	695	12.6	16.3	320/07								
Bamako/Senou	291	12.5	7.9								110/16	

* Interpolated between 1200Z and 1800Z observations.
** Land station reports are at 500/600 m level data, ship reports are at surface.
*** ddd = direction in degrees, ff = speed in knots.

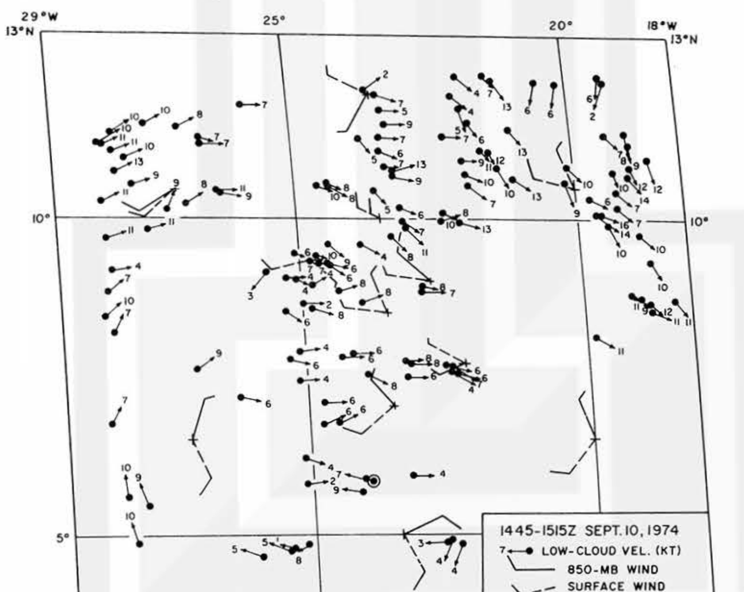

Fig. 6. Low-cloud velocity vectors, total 140, for the period 1445-1515Z, 10 Sept. 1974 computed by McIDAS system. 1500Z or synoptic-time winds are plotted for the surface and 850-mb.

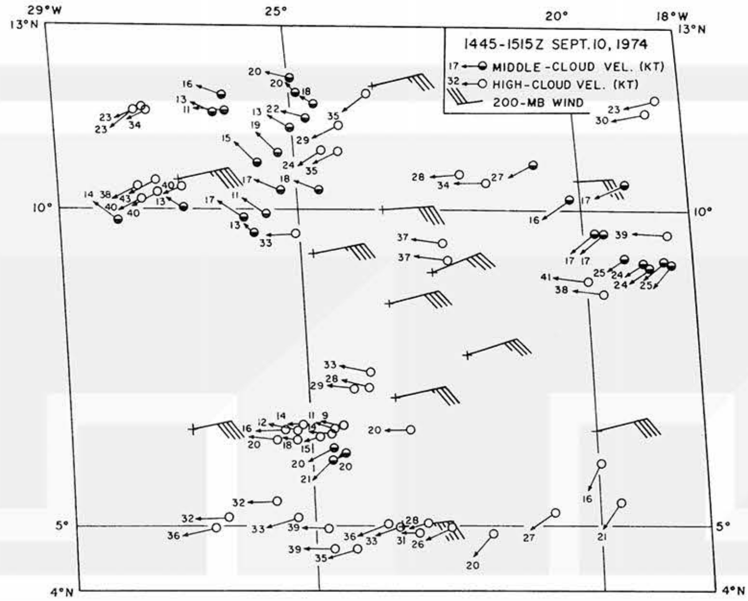

Fig. 7. As in Fig. 6 except for upper-level clouds, total 81, computed by McIDAS system. Middle- and high-clouds are distinguished. Winds plotted are at 200-mb level.

used in McIDAS detect smaller-size cumulus clouds than the 2.0 nmr images could. These smaller-size clouds normally follow the wind near the cloud base and do not have much vertical development. On the other hand, the 2.0 nmr pictures used by METRACOM detect the larger low-level clouds. Such clouds normally exhibit considerable vertical development and, consequently, these tops are the ones tracked. In effect, motions from two low-cloud levels could possibly have been tracked, thus giving rise to dissimilar flow patterns in this particular case.

SOURCES OF ERROR

An assessment of the sources of error in deriving satellite cloud motion and in comparing them with wind observations is appropriate in attempting to draw conclusions from the results of the analyses in this report. Errors in picture registration or navigation which cause fixed geographic points to wander or drift in the picture sequence amounted to a fictitious motion to the southwest at less than 0.5 meter per second for McIDAS (Martin, 1974). In METRACOM, drifting was determined to the west at 1 meter per second. However, this error contribution was corrected in the final computation of each cloud vector. Synoptic-time observations for winds at different levels for 1200 Z and 1800 Z on 10 September 1974 were taken from the GATE 35mm microfilm set of preliminary data, yet unvalidated. It may, therefore, not be representative of all measurements. The data were gathered from the "A" series synoptic chart set. Moreover, linear interpolation is applied to the magnitude and direction of the winds to arrive at the reference time of 1500 Z cloud observation. When this is not possible, either 1200 Z or 1800 Z observation, except calm, is used. Further discrepancy could occur due to the change of the flow between the cloud vector location and the actual balloon location as it drifts from the observing station. Uncertainties of target cloud heights, when compared with some specified levels pose another error. Nonadvective cloud motions would introduce complexities. This feature may remain undetected. Hubert and Whitney (1971) indicate there is no way of measuring the influence of these nonadvective motions. Growth of new cloud elements and the decay of the older clouds are factors that introduce improper targets. Furthermore, it should also be considered that cloud elements may not actually drift with the wind but that it usually blows through the cloud as proposed by Malkus (1958).

PROCEDURES AND ANALYSES

It was originally intended to compare the METRACOM and McIDAS methods by how they performed independently under similar conditions and circumstances, such as identical picture resolutions preferably in the 0.5 nmr visible channel for cloud tracking, a common area and the same reference time of analysis. It may be recalled here that the McIDAS system utilized the 0.5 nmr visible pictures.

When the 0.5 nmr visible ungridded pictures finally became available from the National Climatic Center, a complete set of pictures were subsequently obtained for all four of the five days of operation of the SMS-1 in the 15-minute mode. In evaluating the data, it was observed that picture skewness or drift in the scan line alignment characterized the series. This is evident by observing with reference to the scan line the departure from perpendicularity of the right edge of the picture in Fig. 1. This drift angle varied erratically and considerably in almost all of the pictures examined.

The extent of the variation of this picture skewness is presented in Fig. 8. Time distribution of the skewness factor, whenever it could be measured, for all available 0.5 nmr picture is depicted. The ordinate indicates, in degrees, the amount of left (or right) skewness if the picture appears tilted or slanted to the left (or right). Interspersed in each set are picture images which are not of the 0.5 nmr size. They are classified as not available since they cannot be used in the cloud tracking process. Data concerning the fifth day, 2 September 1974, is not shown since almost all of the available pictures are not measurable for skewness.

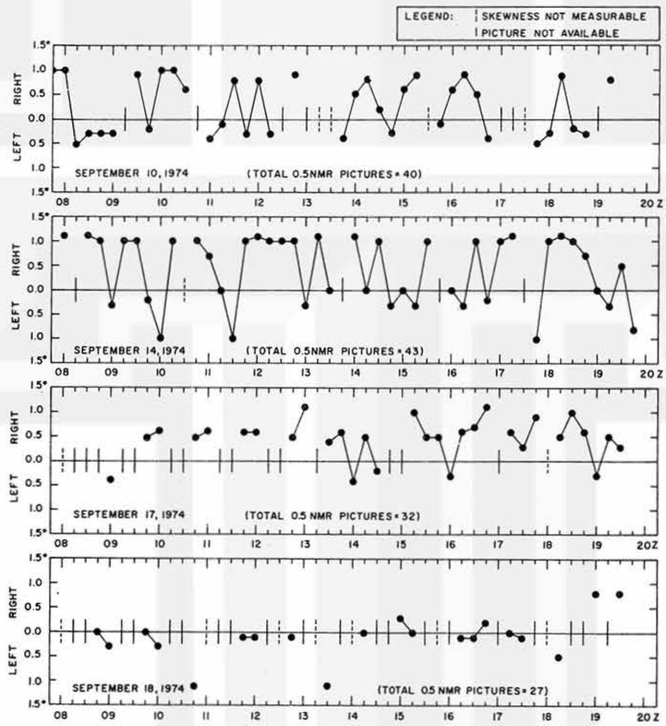

Fig. 8. Time distribution of skewness in degrees for 0.5 nmr visible pictures for 10, 14, 17 and 18, Sept. 1974. A pictures is left- (or right-) skewed if it slants to the left (or right).

At least three successive pictures should comprise the movie loop for cloud tracking in the METRACOM system. In this particular case, the three pictures, time-centered at 1500 Z on 10 September 1974, showed varying skewness. Finding no way to correct it, and inasmuch as the METRACOM technique uses high-quality, dimension-controlled pictures as input, it was decided not to proceed with producing the movie loop for cloud tracking. It was, therefore, considered inappropriate to compare the two methods. No error evaluation for the effects of the irregularity in skewness has been attempted.

Considering that the METRACOM and the McIDAS wind sets had already been produced, it was, nevertheless, deemed advisable to proceed with the evaluation of the analysis. The results, in effect, would no longer reflect on the techniques employed but rather on the effects largely attributable to the combined size-resolution and time-interval factors of the pictures used. Henceforth, reference would no longer be made to the METRACOM or to the McIDAS technique but rather to the 2.0 nmr full-disk, 30-minute-interval picture used by the former or the 0.5 nmr, 15-minute-interval picture image used by the latter, respectively. This evaluation would be particularly interesting inasmuch as the 2.0 nmr visible pictures, heretofore, have been commonly used in the analysis of satellite-derived winds from the earlier geostationary spacecraft, particularly the Applications Technology Satellite (ATS) series. It is obvious that precision is limited to the resolution of the system. However, it would be useful to find out to what extent. This could, perhaps, be one of the first attempts towards that comparison. It should be, however, emphasized that this is just one test case and that two different techniques are employed, although inherent errors therefrom are both within tolerable limits. The effects of the other sources of error have not been isolated inasmuch as they are believed to be of much lesser magnitude and/or contributing towards to the same direction for both analyses.

It was decided to compare the satellite-derived high-cloud motions within a circle of 2 degree-latitude radius of observing stations with wind reports for the upper troposphere and the low-cloud motions within 1.5 degrees for the lower troposphere. Comparison areas have been varied under different circumstances as can be noted in similar studies of satellite-derived cloud motion by Serebreny et al. (1969) and Poteat (1973), among others. The need for sufficient data samples and the consequence resulting from the close proximity of the reference-observing stations in the GATE A/B-scale area were the factors influencing the different sizes of the comparison domain. Such consequence occurs when the same cloud vector becomes eligible to be compared with more than one reference station. Under such circumstances, complexity may arise if sharp circulation changes exist within a comparatively small region. This is especially evident in the lower cloud level.

Resultant cloud-motion vectors and cumulative percentage frequency distributions (cpfd's) are produced. Since more meaningful interpretation of meteorological analysis, in certain instances, result from separate evaluations of wind direction and speed rather than from vector differences, these cpfd's are constructed using absolute differences in cloud direction and speed. The quantitative aspects of the cumulative frequency charts are not discussed since varying synoptic patterns may give different values. Rather, these charts are compared only relatively with each other. Whereas, uncertainties in direction difference occur with calm winds, only observed winds greater than 2 knots are compared with surrounding cloud vectors. Cloud velocities and wind data are compared at different levels.

RESULTS

Shown in Table 2 are two listings of the resultant cloud vectors within designated radii of a wind-reporting station, one for the upper-level and the other for the lower-level cloud for the period centered at 1500 Z on 10 September 1974. The number of sample points within the area of each wind-reporting station is indicated. Interpolated 1500 Z wind data, or the nearest synoptic-time observation, are likewise shown for 200-mb, 850-mb and ocean surfaces.

a) Upper-level Cloud Motion

Figure 9 is a pictorial presentation of the data listed in the upper portion of Table 2. This provides the comparison of the two sets of upper-level cloud motion with the 200-mb winds within the common analysis area. The easterly wind flow pattern is homogeneous. The mean cloud speed is 25 knots and the mean absolute error in direction for the 2.0 nmr cloud velocity analysis is 18 degrees. For the 0.5 nmr analysis it is 28 knots and 16 degrees, respectively.

Table 2. Summary of Resultant Cloud Vectors and Wind Observations at Various Levels on 10 September 1974.

a) Cloud vectors within 2-degrees latitude of wind observation.

LOCATION		1500Z Wind 200-MB		UPPER-LEVEL CLOUD VELOCITY					
				2.0 nmr Image			0.5 nmr Image		
°N	°W	Dir(°)	Spd(Kt)	No. in Sample	Dir(°)	Spd(Kt)	No. in Sample	Dir(°)	Spd(Kt)
12.0	23.5	077	32	6	084	24	5	066	30
10.5	27.0	080	42	5	080	25	8	063	38
10.5	20.0	085	28	5	066	27	7	092	33
10.0	23.5	087	38	9	080	23	9	080	31
9.3	24.8	080	41	6	079	20	2	064	30
9.0	22.7	*070	*37	8	059	25	6	096	34
8.5	23.5	077	40	7	062	24	7	097	31
7.7	22.2	075	35	9	060	25	6	099	31
7.0	23.5	080	31	10	060	25	13	097	18
6.5	27.0	082	39	6	070	27	11	087	22
6.5	20.0	077	40	9	050	26	3	044	21
5.0	23.5	085	41	9	048	24	16	080	26
		TOTAL		89			92		

b) Cloud vectors within 1.5-degrees latitude of wind observation.

LOCATION		1500Z Wind				LOWER-LEVEL CLOUD VELOCITY					
		850-MB		Ocean Surface		2.0 nmr Image			0.5 nmr Image		
°N	°W	Dir(°)	Spd(Kt)	Dir(°)	Spd(Kt)	No. in Sample	Dir(°)	Spd(Kt)	No. in Sample	Dir(°)	Spd(Kt)
12.0	23.5	215	05	300	04	6	350	12	14	284	06
10.5	27.0	240	09	*230	*08	15	329	09	18	251	09
10.5	20.0	340	05	285	10	7	029	15	18	323	10
10.0	23.5	295	07	295	08	20	344	09	26	290	07
9.3	24.8	130	02	260	07	13	346	10	22	291	05
9.0	22.7	*315	*09	280	05	6	343	11	18	289	07
8.5	23.5	340	06	280	04	12	353	10	24	287	06
7.7	22.2	250	05	*300	*02		No Vector		9	281	06
7.0	23.5	320	05	**230	**08	1	027	12	16	273	06
6.5	27.0	*020	*04	155	08	2	057	12	5	200	06
6.5	20.0	340	04	220	08		No Vector			No Vector	
5.0	23.5	067	08	155	09	2	065	16	7	077	03
				TOTAL		84			177		

nmr = nautical mile resolution
* 1200Z observation
** 1800Z observation

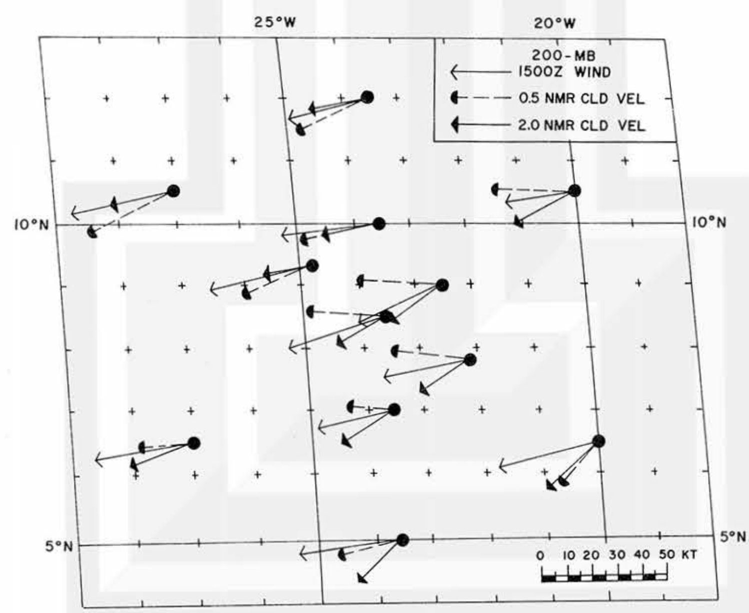

Fig. 9. Resultant high-cloud motions from 0.5 and 2.0 nmr mode pictures together with 200-mb winds at 1500Z, 10 Sept. 1974.

It appears, thus, that the upper-level analyses are reasonably consistent with each other, regardless of ground resolution and time-interval factors concerned. Both show very nearly the same degree of error distribution in direction and are within 3 knots difference in speed, in the mean. The 2.0 nmr cloud vector computation shows slower speed. Further, it indicates that wind speeds at this level, in most all cases, are stronger than the cloud speeds. This was also observed in the southern hemisphere by Salomonson (1975). Figure 10 depicts the cpfd of the absolute difference in direction and speed of the computed high-cloud motion within 2 degrees latitude radius of the 1500 Z winds at 200-mb for both 0.5 and 2.0 nmr analyses. This illustrates that direction differences up to the upper quartile range are almost identical for both cases. And since the former has stronger winds on the average, the speed difference curves are reflected as such. N is the total number in the sample data.

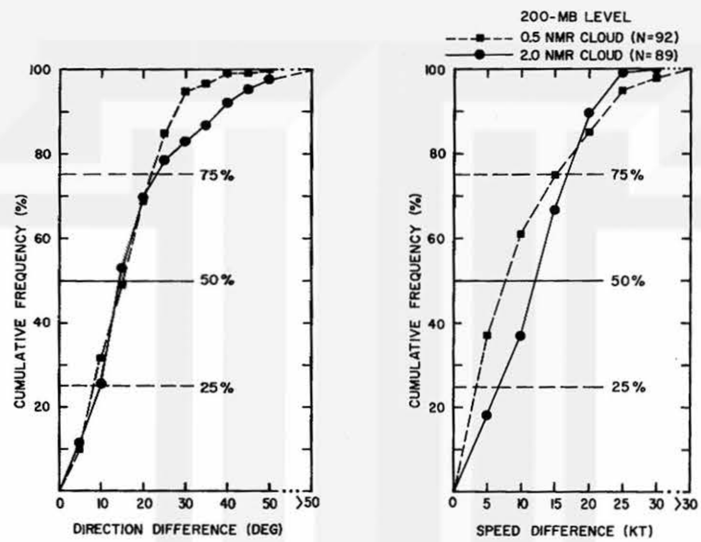

Fig. 10. Cumulative percentage frequency distributions of absolute differences in direction and speed for high-cloud motions within 2-degrees radius of 200-mb winds at 1500Z, 10 Sept. 1974 from 0.5 and 2.0 nmr cloud analyses over the common area. N is the sample size.

b) Lower-level cloud motion

The resultant cloud motion vectors plotted with the 850-mb winds at 1500 Z appear in Fig. 11. A general anticyclonic flow is depicted by each set of vectors. The 2.0 nmr cloud velocities indicate curvature of longer radius than the others. It also shows relatively stronger winds. Figure 12 compares the cpfd's when referred to the

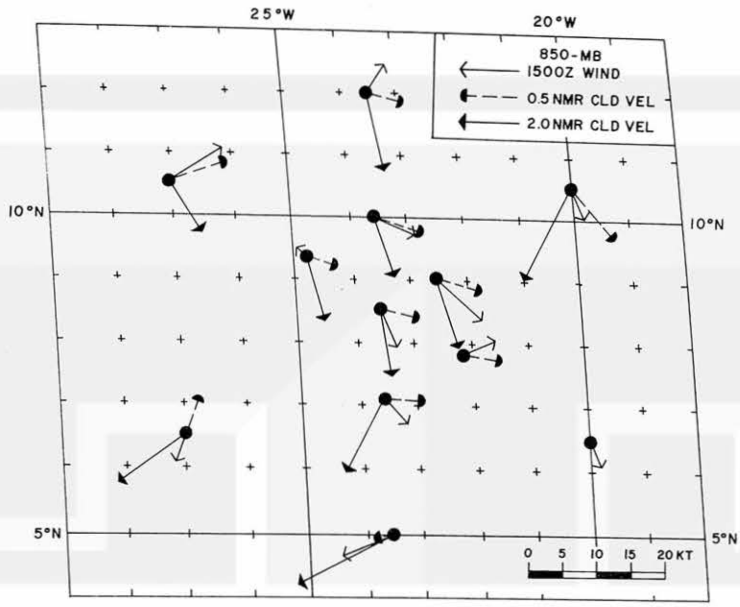

Fig. 11. As in Fig. 9 except for 850-mb winds.

850-mb winds. It appears that the 0.5 nmr cloud velocities show less error in both direction and speed than that of the 2.0 nmr cloud analysis.

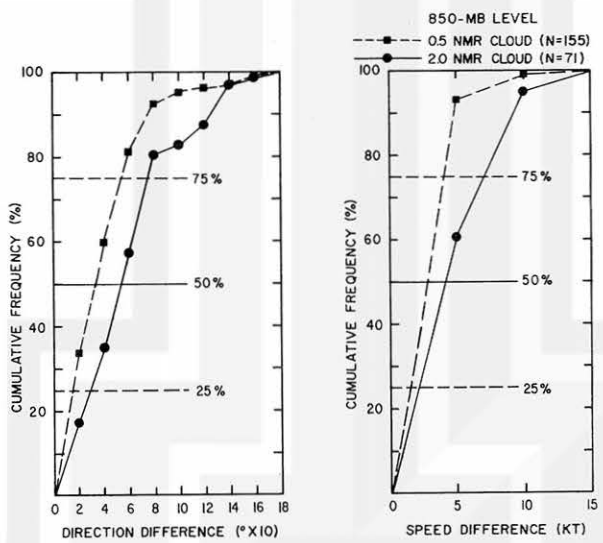

Fig. 12. As in Fig. 10 except within 1.5-degrees of 850-mb winds.

When the same resultant cloud vectors are plotted with the surface winds at 1500 Z, the flow field is visualized in Fig. 13. Anticyclonic flow is still evident in both analyses. Again the 2.0 nmr cloud velocities describe a wider arc and relatively

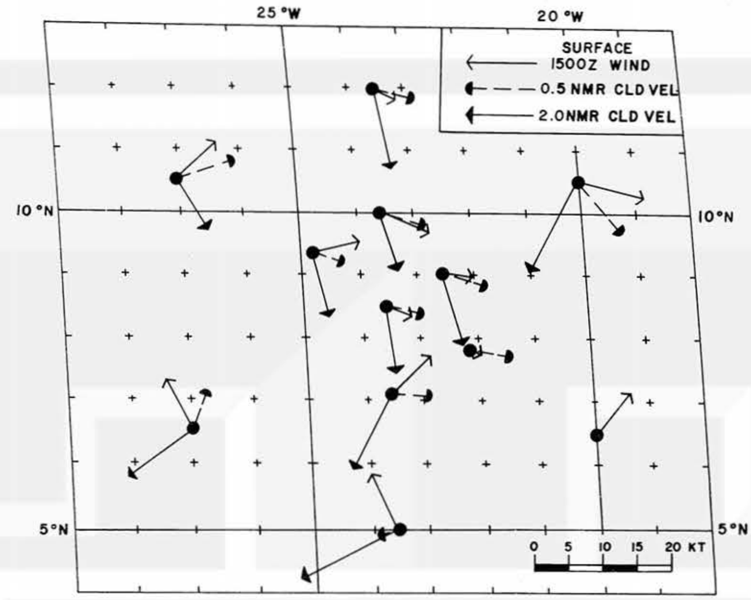

Fig. 13. As in Fig. 9 except for surface winds.

stronger winds than the others. A weak but closed anticyclonic circulation can fit the flow pattern of the 0.5 nmr cloud analysis and the surface winds. Fig. 14 shows the better representation by the 0.5 nmr cloud analysis to approximate the surface wind flow than the 2.0 nmr cloud vectors. In reviewing the cpfd's in Figs. 12 and 14, it can be noted the larger range of discrepancies in wind direction and smaller range in

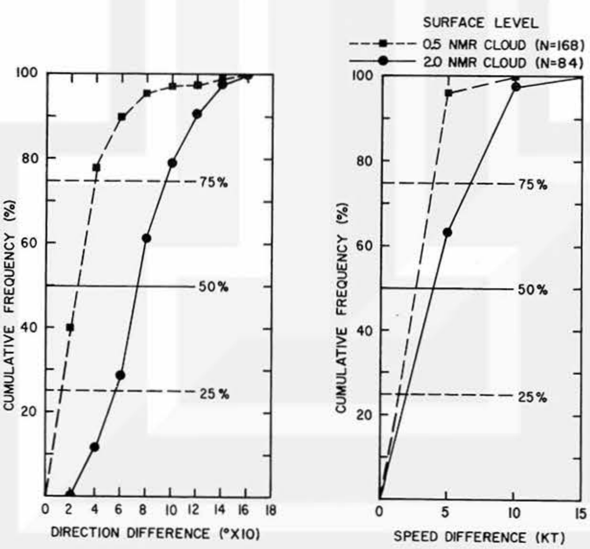

Fig. 14. As in Fig. 12 except for surface winds.

wind speed for the lower-level cloud comparisons. These are due to variable wind direction and weak wind speed. There are more sample points in the 0.5 nmr cloud analysis than in the 2.0 nmr mode.

It now may become interesting to find out at what level, whether at the surface or at 850-mb, the 0.5 nmr cloud velocities make a better fit with the wind flow. Referring to Fig. 15, where the cpfd's of the 0.5 nmr low clouds are displayed with the 850-mb and the surface winds, it appears that the cloud tracers better fit the surface wind flow.

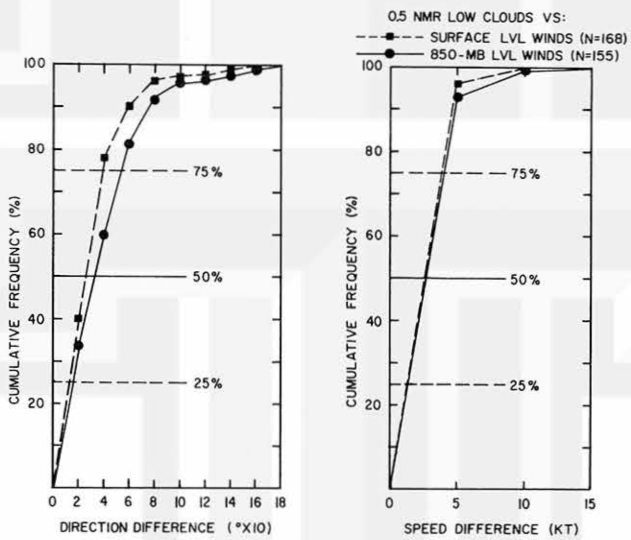

Fig. 15. Cumulative percentage frequency distributions of absolute differences in direction and speed for low-cloud motion vs. surface winds and also vs. 850-mb winds at 1500Z, 10 Sept. 1974 from 0.5 nmr, 15-minute interval pictures.

Insofar as the 2.0 nmr cloud vectors are concerned, the comparison of the cpfd's in Fig. 16 tends to show better approximation of wind flow at or near the 850-mb level than at the surface. The results shown in Fig. 17, which is similar to the preceding figure except that more sample points are traced from the larger analysis area. better evidence (see area A in Fig. 2 and also Fig. 4).

CONCLUSIONS

Computations of cloud-motion vectors over the area of the GATE A/B-scale ship network for 10 September 1974 centered at 1500 Z were performed independently

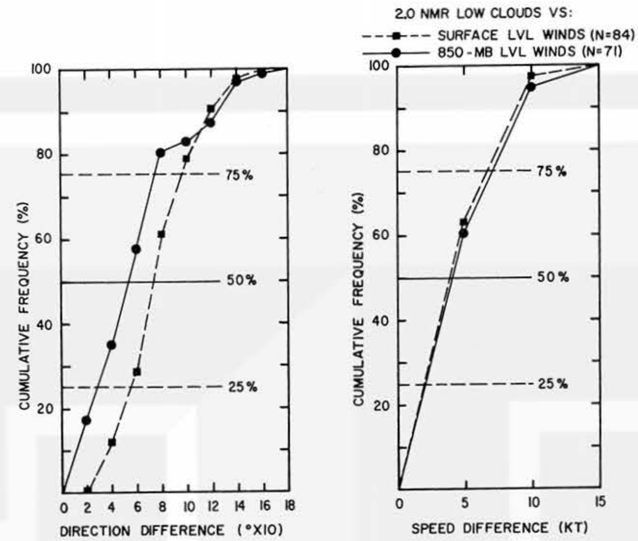

Fig. 16. As in Fig. 15 except for 2.0 nmr full-disk, 30-minute interval pictures.

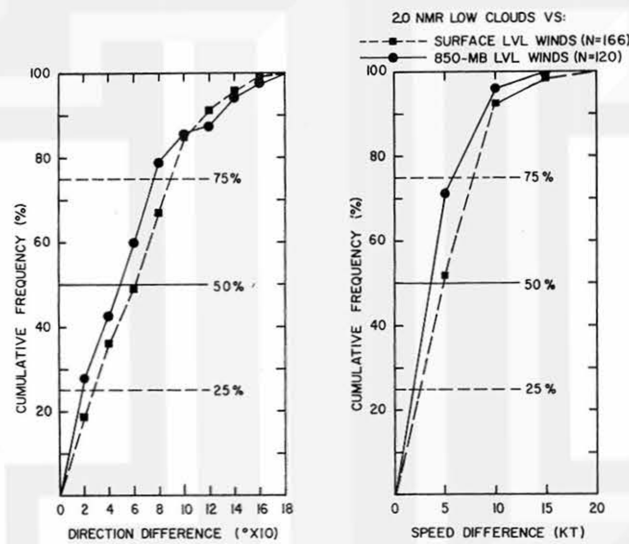

Fig. 17. As in Fig. 16 except for the overall area shown in Fig. 3 for the 2.0 nmr mode pictures.

by the University of Wisconsin using its McIDAS scheme and by the University of Chicago through its METRACOM technique. It was intended to assess the results of these techniques using picture images with identical image subpoint resolution and time-interval frequency. However, McIDAS utilized the 0.5 nmr, 15-minute interval film images with processing done on original digitized data, while METRACOM used the 2.0 nmr full-disk, 30-minute interval pictures only available then. When the 0.5 nmr series were obtained, it was observed that skewness of irregular magnitudes characterized the sets. Finding no way to correct it, and inasmuch as the METRACOM technique uses high-quality, dimension-controlled pictures as input, it was considered inappropriate to compare the two methods.

Consequently, comparison is now aimed at assessing the results of the analyses when different characteristics of size-resolution and time-interval frequency of the pictures are simultaneously involved. This attempt could be particularly interesting inasmuch as the 2.0 nmr full-disk, 30-minute interval visible pictures, heretofore, have been commonly used in the analysis of satellite-derived winds from the earlier geostationary spacecraft, particularly the ATS series.

The results are summarized as follows:

a) The upper-level cloud motions derived from both analyses closely agree in direction with the 200-mb level winds. The computed cloud speeds are both slower than the wind observations. The 2.0 nmr mode pictures showed slower cloud speeds than the 0.5 nmr mode by about 3 knots on the average.

b) The lower-level cloud motions derived from the 0.5 nmr film images closely approximate the surface wind flow. Cloud motions derived from the 2.0 nmr pictures tend to depict the wind pattern at the 850-mb level better than the surface winds. This level also conforms with that suggested by Izawa and Fujita (1969) from analysis of pictures obtained by ESSA and ATS. No comparison is available with other wind levels in between this layer. The different levels which fit the low-cloud motions from analysis of the 0.5 and 2.0 nmr mode pictures could possibly be due to the different levels of the low-clouds detected and tracked from pictures taken with different ground resolution cameras. The 0.5 nmr pictures detect smaller-size cumulus clouds than the 2.0 nmr images could. These smaller-size clouds normally follow the wind near the cloud base and do not have much vertical development. On the other hand, the 2.0 nmr pictures detect the larger low-level clouds. Such clouds normally exhibit considerable vertical development and, consequently, these tops are the ones tracked. Cloud speeds computed from 2.0 nmr pictures are a trifle faster than the wind observations and the 0.5 nmr mode analysis. The quantitative aspects of the low-cloud evaluation are not presented in this report; varying synoptic conditions may give different values.

c) Between utilizing picture images in the 0.5 and 2.0 nmr modes, it is found that the former provides better fit with the wind data at lower levels, both at the surface and at 850-mb.

d) Under the synoptic conditions prevailing in the lower troposphere at that time, i.e., the prevalence of small fair weather trade cumuliform clouds, the 0.5 nmr, 15-minute interval pictures, indeed, provided more data points and better-quality, easier-recognized tracer cloud images than the 2.0 nmr full-disk, 30-minute interval pictures in the same area zoomed in.

It is suggested that additional studies be conducted under other synoptic situations for further comparison.

ACKNOWLEDGEMENTS

Counterpart arrangements and special efforts in the initial attempt to jointly assess the results of the cloud-motion analyses were generously provided by Dr. David W. Martin and Prof. Verner E. Suomi of the University of Wisconsin. Sincere thanks are due them, particularly for supplying the wind sets computed by the McIDAS and for their permission to use same in this research report.

REFERENCES

Chang, Y. M., J. J. Tecson and T. T. Fujita, 1973: METRACOM System of Cloud-Velocity Determination from Geostationary Satellite Pictures. SMRP Research Paper 110, The University of Chicago.

Chatters, G. C. and V. E. Suomi, 1975: The Applications of McIDAS. IEEE Transactions on Geoscience Electronics, GE-13, 137-146.

Houghton, D. D. and D. E. Parker, 1974: The Synoptic-Scale Sub-Programme of GATE. GATE Report No. 6, Geneva, ICSU/WMO.

Hubert, L. F. and L. F. Whitney, Jr., 1971: Wind Estimation from Geostationary-Satellite Pictures. Mon. Wea. Rev., 99, 665-672.

Izawa, T. and T. Fujita, 1969: Relationship Between Observed Winds and Cloud Velocities Determined from Pictures Obtained by the ESSA III, ESSA V and ATS 1 Satellites. COSPAR Space Research IX, Proceed. of Open Meetings of Working Groups of the Eleventh Plenary Meeting of COSPAR. Tokyo, 9-21 May 1968, 571-579.

ISMG Group, 1975. Report on the Field Phase of GATE - Meteorological Atlas. GATE Report No. 17, Geneva, ICSU/WMO.

Malkus, J. S., 1958: On the Structure of the Trade Wind Moist Layer. Papers Phys. Oceanogr. Meteor., 13.

Martin, D. W., University of Wisconsin, 1974: (Personal Communication)

Poteat, K. O., 1973: A Comparison of Satellite-Derived, Low-Level and Cirrus-Level Winds with Conventional Wind Observations. Jour. Appl. Meteor., 12, 1416-1419.

Salomonson, V. V., 1975: EOLE Balloons and ATS Cloud Motion Comparisons. Jour. Appl. Meteor., 14, 1266-1270.

Serebreny, S. M., R. G. Hadfield, R. M. Trudeau and E. J. Wiegman, 1969: Comparison of Cloud Motion Vectors and Rawinsonde Data. Final Report. Stanford Research Institute, Menlo Park, California.

Smith, E. A., 1975: The McIDAS System. IEEE Transactions on Geoscience Electronics, GE-13, 123-136.

Suomi, V. E. (Principal Investigator), 1975: Man-Computer Interactive Data Access System (McIDAS). Final Report Contract NAS5-23296, University of Wisconsin, Madison.

MESOMETEOROLOGY PROJECT - - - RESEARCH PAPERS

(Continued from front cover)

42.* A Study of Factors Contributing to Dissipation of Energy in a Developing Cumulonimbus - Rodger A. Brown and Tetsuya Fujita

43. A Program for Computer Gridding of Satellite Photographs for Mesoscale Research - William D. Bonner

44. Comparison of Grassland Surface Temperatures Measured by TIROS VII and Airborne Radiometers under Clear Sky and Cirriform Cloud Conditions - Ronald M. Reap

45. Death Valley Temperature Analysis Utilizing Nimbus I Infrared Data and Ground-Based Measurements - Ronald M. Reap and Tetsuya Fujita

46. On the "Thunderstorm-High Controversy" - Rodger A. Brown

47. Application of Precise Fujita Method on Nimbus I Photo Gridding - Lt. Cmd. Ruben Nasta

48. A Proposed Method of Estimating Cloud-top Temperature, Cloud Cover, and Emissivity and Whiteness of Clouds from Short- and Long-wave Radiation Data Obtained by TIROS Scanning Radiometers - T. Fujita and H. Grandoso

49. Aerial Survey of the Palm Sunday Tornadoes of April 11, 1965 - Tetsuya Fujita

50. Early Stage of Tornado Development as Revealed by Satellite Photographs - Tetsuya Fujita

51. Features and Motions of Radar Echoes on Palm Sunday, 1965 - D. L. Bradbury and T. Fujita

52. Stability and Differential Advection Associated with Tornado Development - Tetsuya Fujita and Dorothy L. Bradbury

53. Estimated Wind Speeds of the Palm Sunday Tornadoes - Tetsuya Fujita

54. On the Determination of Exchange Coefficients: Part II - Rotating and Nonrotating Convective Currents - Rodger A. Brown

55. Satellite Meteorological Study of Evaporation and Cloud Formation over the Western Pacific under the Influence of the Winter Monsoon - K. Tsuchiya and T. Fujita

56. A Proposed Mechanism of Snowstorm Mesojet over Japan under the Influence of the Winter Monsoon - T. Fujita and K. Tsuchiya

57. Some Effects of Lake Michigan upon Squall Lines and Summertime Convection - Walter A. Lyons

58. Angular Dependence of Reflection from Stratiform Clouds as Measured by TIROS IV Scanning Radiometers - A. Rabbe

59. Use of Wet-beam Doppler Winds in the Determination of the Vertical Velocity of Raindrops inside Hurricane Rainbands - T. Fujita, P. Black and A. Loesch

60. A Model of Typhoons Accompanied by Inner and Outer Rainbands - Tetsuya Fujita, Tatsuo Izawa., Kazuo Watanabe and Ichiro Imai

61. Three-Dimensional Growth Characteristics of an Orographic Thunderstorm System - Rodger A. Brown

62. Split of a Thunderstorm into Anticyclonic and Cyclonic Storms and their Motion as Determined from Numerical Model Experiments - Tetsuya Fujita and Hector Grandoso

63. Preliminary Investigation of Peripheral Subsidence Associated with Hurricane Outflow - Ronald M. Reap

64. The Time Change of Cloud Features in Hurricane Anna, 1961, from the Easterly Wave Stage to Hurricane Dissipation - James E. Arnold

65. Easterly Wave Activity over Africa and in the Atlantic with a Note on the Intertropical Convergence Zone during Early July 1961 - James E. Arnold

66. Mesoscale Motions in Oceanic Stratus as Revealed by Satellite Data - Walter A. Lyons and Tetsuya Fujita

67. Mesoscale Aspects of Orographic Influences on Flow and Precipitation Patterns - Tetsuya Fujita

68. A Mesometeorological Study of a Subtropical Mesocyclone -Hidetoshi Arakawa, Kazuo Watanabe, Kiyoshi Tsuchiya and Tetsuya Fujita

69. Estimation of Tornado Wind Speed from Characteristic Ground Marks - Tetsuya Fujita, Dorothy L. Bradbury and Peter G. Black

70. Computation of Height and Velocity of Clouds from Dual, Whole-Sky, Time-Lapse Picture Sequences - Dorothy L. Bradbury and Tetsuya Fujita

71. A Study of Mesoscale Cloud Motions Computed from ATS-I and Terrestrial Photographs - Tetsuya Fujita, Dorothy L. Bradbury, Clifford Murino and Louis Hull

72. Aerial Measurement of Radiation Temperatures over Mt. Fuji and Tokyo Areas and Their Application to the Determination of Ground- and Water-Surface Temperatures - Tetsuya Fujita, Gisela Baralt and Kiyoshi Tsuchiya

73. Angular Dependence of Reflected Solar Radiation from Sahara Measured by TIROS VII in a Torquing Maneuver - Rene Mendez.

74. The Control of Summertime Cumuli and Thunderstorms by Lake Michigan During Non-Lake Breeze Conditions - Walter A. Lyons and John W. Wilson

75. Heavy Snow in the Chicago Area as Revealed by Satellite Pictures - James Bunting and Donna Lamb

76. A Model of Typhoons with Outflow and Subsidence Layers - Tatsuo Izawa

77. Yaw Corrections for Accurate Gridding of Nimbus HRIR Data - R. A. Madden

78. Formation and Structure of Equatorial Anticyclones caused by Large-Scale Cross Equatorial Flows determined by ATS I Photographs - T. T. Fujita, K. Watanabe and T. Izawa

79. Determination of Mass Outflow from a Thunderstorm Complex using ATS III Pictures - T. T. Fujita and D. L. Bradbury

80. Development of a Dry Line as shown by ATS Cloud Photography and verified by Radar and Conventional Aerological Data - D. L. Bradbury

81. Dynamical Analysis of Outflow from Tornado-Producing Thunderstorms as revealed by ATS III Pictures - K. Ninomiya

*82. Computation of Cloud Heights from Shadow Positions through Single Image Photogrammetry of Apollo Pictures - T. T. Fujita

83. Aircraft, Spacecraft, Satellite and Radar Observations of Hurricane Gladys, 1968 - R. C. Gentry, T. Fujita and R. C. Sheets

84. Basic Problems on Cloud Identification related to the design of SMS-GOES Spin Scan Radiometers - T. T. Fujita

85. Mesoscale Modification of Synoptic Situations over the Area of Thunderstorms' Development as revealed by ATS III and Aerological Data - K. Ninomiya

86. Palm Sunday Tornadoes of April 11, 1965 - T. T. Fujita, D. L. Bradbury and C. F. Van Thullenar (Reprinted from Mon. Wea. Rev., 98, 29-69, 1970)

SATELLITE AND MESOMETEOROLOGY RESEARCH PROJECT --- PAPERS

87. Patterns of Equivalent Blackbody Temperature and Reflectance of Model Clouds computed by changing Radiometer's Field of View - J. J. Tecson
88. Lubbock Tornadoes of 11 May 1970 - T. T. Fujita
89. Estimate of Areal Probability of Tornadoes from Inflationary Reporting of their Frequencies - T. T. Fujita
90. Application of ATS III Photographs for determination of Dust and Cloud Velocities over Northern Tropical Atlantic - T. T. Fujita
91. A Proposed Characterization of Tornadoes and Hurricanes by Area and Intensity - T. T. Fujita
92. Estimate of Maximum Wind Speeds of Tornadoes in Three Northwestern States - T. T. Fujita
93. In- and Outflow Field of Hurricane Debbie as revealed by Echo and Cloud Velocities from Airborne Radar and ATS-III Pictures - T. T. Fujita and P. G. Black (Reprinted from Preprint of Radar Meteorology Conference, Nov. 17-20, 1970, Tucson, Arizona)
94. Characterization of 1965 Tornadoes by their Area and Intensity - J. J. Tecson
*95. Computation of Height and Velocity of Clouds over Barbados from a Whole-Sky Camera Network - R. D. Lyons
96. The Filling over Land of Hurricane Camille, August 17-18, 1969 - D. L. Bradbury
97. Tornado Occurrences related to Overshooting Cloud-Top Heights as determined from ATS Pictures - T. T. Fujita
98. FPP Tornado Scale and its Applications - T. T. Fujita and A. D. Pearson
99. Preliminary Results of Tornado Watch Experiment 1971 - T. T. Fujita, J. J. Tecson and L. A. Schaal
100. F-Scale Classification of 1971 Tornadoes - T. T. Fujita
101. Typhoon-Associated Tornadoes in Japan and new evidence of Suction Vortices in a Tornado near Tokyo - T. T. Fujita
102. Proposed Mechanism of Suction Spots accompanied by Tornadoes - T. T. Fujita
103. A Climatological Study of Cloud Formation over the Atlantic during Winter Monsoon - H. Shitara
**104. Statistical Analysis of 1971 Tornadoes - E. W. Pearl
105. Estimate of Maximum Windspeeds of Tornadoes in Southernmost Rockies - T. T. Fujita
106. Use of ATS Pictures in Hurricane-Modification - T. T. Fujita
107. Mesoscale Analysis of Tropical Latin America - T. T. Fujita
108. Tornadoes Around The World - T. T. Fujita (Reprinted from Weatherwise, 26, No. 2, April 1973)
109. A Study of Satellite-Observed Cloud Patterns of Tropical Cyclones - E. E. Balogun
110. METRACOM System of Cloud-Velocity determination from Geostationary Satellite Pictures - Y. M. Chang, J. J. Tecson and T. T. Fujita
111. Proposed Mechanism of Tornado Formation from Rotating Thunderstorm - T. T. Fujita
112. Joliet Tornado of April 6, 1972 - E. W. Pearl
113. Results of FPP Classification of 1971 and 1972 Tornadoes - T. T. Fujita and A. D. Pearson
114. Satellite-Tracked Cumulus Velocities - T. T. Fujita, E. W. Pearl and W. E. Shenk
115. General and Local Circulation of Mantle and Atmosphere toward Prediction of Earthquakes and Tornadoes - T. T. Fujita and K. Fujita
116. Cloud Motion Field of Hurricane Ginger during the Seeding Period as determined by the METRACOM System - J. J. Tecson, Y. M. Chang and T. T. Fujita
117. Overshooting Thunderheads observed from ATS and Learjet - T. T. Fujita
118. Thermal and Dynamical Features of a Thunderstorm with a Tilted Axis of Rotation - T. T. Fujita
119. Characteristics of Anvil-Top Associated with the Poplar Bluff Tornado of May 7, 1973 - E. W. Pearl
120. Jumbo Tornado Outbreak of 3 April 1974 - T. T. Fujita
121. Cloud Velocities Over The North Atlantic Computed From ATS Picture Sequences - Y. M. Chang and J. J. Tecson
122. Analysis of Anvil Growth for ATS Pictures - Y. M. Chang
**123. Evaluation of Tornado Risk Based on F-Scale Distribution - E. W. Pearl
124. Superoutbreak Tornadoes Of April 3, 1974 As Seen In ATS Pictures - T. T. Fujita and G. S. Forbes
125. Kinematic Analysis of Tropical Storm Based On ATS Cloud Motions - J. J. Tecson and T. T. Fujita
126. Overshooting Top Behavior of Three Tornado-Producing Thunderstorms - T. A. Umenhofer
127. New Evidence from April 3-4, 1974 Tornadoes - T. T. Fujita
128. Long-Term Fluctuation of Tornado Activities - T. T. Fujita, A. Pearson and D. M. Ludlum
129. Relationship between Tornadoes and Hook Echoes on April 3, 1974 - G. S. Forbes
130. Cloud-Top Parameters - A Hail Indicator - E. W. Pearl, W. E. Shenk and W. Skillman
131. Detection of Severe Storms by Satellites - T. T. Fujita
**132. The Gothenburg Tornado Family of June 18, 1975 - G. S. Forbes
133. Analysis and Use of Meteorological Data: An Outline prepared for UN/WMO Regional Training Seminar (Nairobi) - T. T. Fujita
134. A Profile of an Easterly Wave from SMS Photographs and GATE Ship Reports - J. J. Tecson and E. E. Balogun.
135. Description of Mesoscale Systems - E. W. Pearl.